

# NUMERICAL ANALYSIS OF FATIGUE DAMAGE BEHAVIOR IN FIBER COMPOSITES UNDER DIFFERENT BLOCK LOADING CONDITIONS

M. Brod<sup>1,\*</sup>, A. Dean<sup>1,2</sup>, S. Scheffler<sup>1</sup>, M. Bishara<sup>1</sup>, R. Rolfes<sup>1</sup>

<sup>1</sup> Leibniz University Hannover, Institute of Structural Analysis, Appelstraße 9A, 30167 Hannover, Germany

<sup>2</sup> School of Civil Engineering, College of Engineering, Sudan University of Science and Technology, P.O. Box 72, Khartoum, Sudan

\* m.brod@isd.uni-hannover.de

**Keywords:** Unidirectional fiber composites, Fatigue damage modeling, Block loading.

**Summary:** *This contribution focuses on the application of a progressive fatigue damage model (FDM) for life prediction of unidirectional carbon fiber composites under variable block loading conditions. First, the proposed modeling approach and its main calculation steps are presented. Here, it is explained which model extensions were made in order to be able to reliably perform fatigue analyses under variable block loading patterns. Second, results of finite element simulations (which were carried out using the FDM) for multidirectional laminates under different loading conditions were presented. Thereby, in addition to load sequences with variable amplitudes, block loading patterns with combined tensile and compressive loads were considered. Finally, the extended FDM was applied for damage prediction on a fuselage shell of a blended wing body aircraft in order to demonstrate the model applicability to structural use cases. All results presented in this study were critically examined for their plausibility. In particular, the comparison of the simulations with experimental data for the block loading investigations demonstrates the validity of the proposed FDM.*

## 1. INTRODUCTION

In rotating and moving structural components, where a particularly high degree of lightweight design is required, fiber-reinforced plastics (FRP) play a central role. Excellent specific stiffness and strength properties of FRP offer advantages over conventional metallic materials. In service, FRP structures usually experience random cyclic loading with variable load characteristics (including different stress amplitudes and load orientations). This activates damage mechanisms in the component that induce material degradation and consequent performance losses. Another advantage of multidirectional FRP is their capability to carry very high loads even if cracks or a damage are present. In the aerospace industry, damage tolerance concepts [1] are generally used when developing safety-relevant components. This involves tolerating existing material damage until it is repaired during maintenance. In order to be able to plan optimum maintenance intervals, it is mandatory to estimate the damage development under variable

cyclic load conditions as accurately as possible. Along with cost-intensive tests on prototypes, detailed and reliable modeling tools are used in the development process. However, fatigue models used in industry are often too inaccurate (no consideration of load sequence effects, stress redistribution, specific damage mechanisms, etc.), which leads to an over- or underestimation of the lifetime. Although a variety of promising fatigue models [2] have been proposed in recent years, none has established itself as a "standard model" compared to static strength models (e.g. Puck or Hashin). Therefore, this contribution focuses on presenting a layer- and energy-based fatigue damage model [3] (hereafter referred to as FDM) for unidirectional FRP and its application for fatigue analysis under different loading conditions. The advantages of the proposed FDM include its ability to account for different damage modes as well as stress redistribution and load sequence effects under complex loading situations [4–6]. The first part of this paper is devoted to explaining the basic functionality of the FDM and its application to variable block loading conditions. Based on this, results of fatigue simulations performed on multidirectional laminates for different block loading patterns are presented. The third part of the paper demonstrates the applicability of the extended FDM on structural use cases. In this context, a fatigue analysis of a blended wing body fuselage shell was performed considering a standardized aircraft load spectrum. Finally, the results obtained in this study are summarized and some concluding remarks are given.

## 2. A PROGRESSIVE FATIGUE DAMAGE MODEL FOR FIBER COMPOSITES

The FDM presented in this section is designed for unidirectional FRP composites and can be applied from coupon- to component-level. The model includes a nonlinear damage accumulation law and analyzes the damage evolution in each layer of the laminate (layer-based approach). The nonlinear damage accumulation law allows to account for load-sequence effects, typical for FRP composites, whereas the layer-based analysis allows to capture complex load-redistribution effects. Additionally, in case of static failure during the fatigue analysis, material properties are degraded according to the mode-discrete Puck fracture theory. The FDM has been implemented as a user-defined material subroutine (UMAT) in the commercial finite element software ABAQUS/Implicit. The model is based on the assumption of a transversal-isotropic material behavior. In relation to the local material orientations  $j$  and the applied loads  $k$ , strength and stiffness degradation factors are introduced ( $\eta_{R_j^k}$  and  $\eta_{E_j^k}$ , respectively), which describe the state of damage for each Gauss Point of the FE-model. The degraded stiffness and strength parameters ( $E_{j,da}^k$  and  $R_{j,da}^k$ , respectively) can be expressed as follows:

$$E_{j,da}^k = \eta_{E_j^k} \cdot E_j^k, \text{ and } R_{j,da}^k = \eta_{R_j^k} \cdot R_j^k, \quad (1)$$

where  $\eta_{R_j^k, E_j^k} = 0$  represents complete damage and  $\eta_{R_j^k, E_j^k} = 1$  the pristine material state. The main feature of the FDM is the application of an energy-based damage hypothesis [7], originally developed for the fatigue analysis of reinforced concrete. This hypothesis implies that the state of damage under static loading is comparable with the state of fatigue damage

under cyclic loading, if the amount of energy  $g_j^k$  dissipated by a material point for both loading scenarios is equal. When adopting this hypothesis to FRP, the damage state of a certain material orientation  $j$  depends only on the amount of energy dissipated in this orientation. Consequently, the damage state in relation to stiffness and strength properties is comparable ( $g_j^{st,k} = g_j^{fat,k} \rightarrow E_{j,da}^{st,k} = E_{j,da}^{fat,k}$ , and  $R_{j,da}^{st,k} = R_{j,da}^{fat,k}$ ). The application of this energy hypothesis also allows the fatigue analysis to be performed load-block-wise, thus bypassing a time-consuming and computationally intensive cycle-by-cycle analysis.

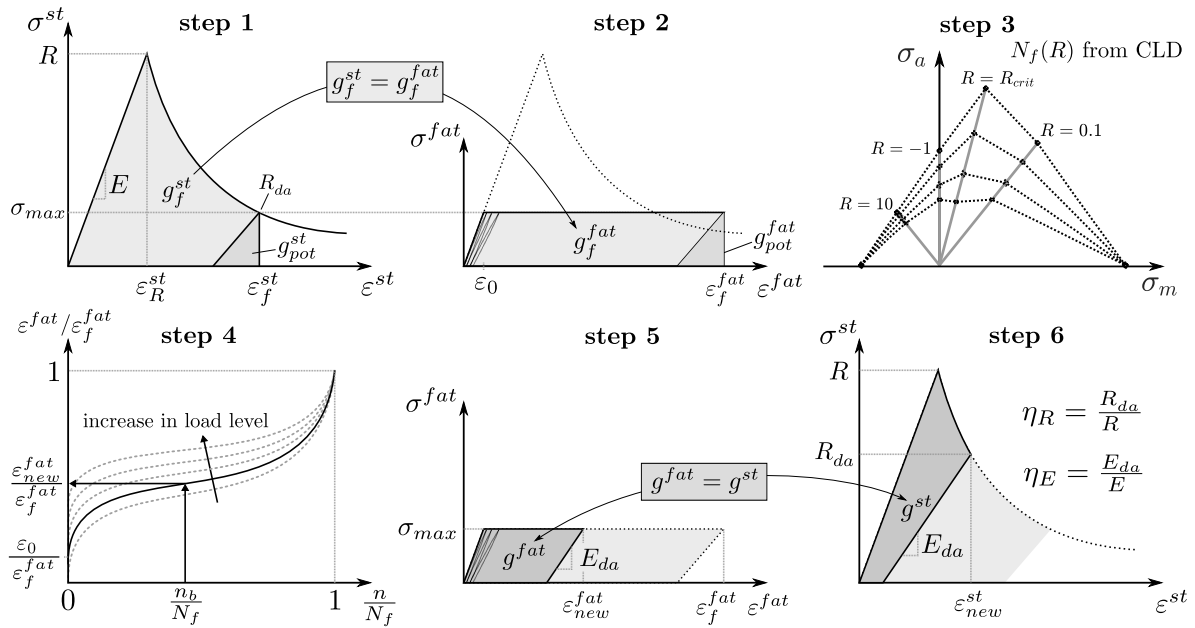


Figure 1. Schematic illustration of determining stiffness ( $\eta_E$ ) and strength ( $\eta_R$ ) degradation factors. Steps 1 and 2: characterization of the failure state by means of stress-strain curves; step 3: determination of the number of load cycles to failure  $N_f$  by means of constant life diagrams (CLD); step 4: strain evolution  $\varepsilon_{new}^{fat}$  for the current load block  $n_b$ ; steps 5 and 6: accumulation of dissipated energy and determination of the updated degradation factors  $\eta_E$  and  $\eta_R$ .

Figure 1 explains the main steps during the damage calculation procedure. In steps 1 and 2, the ultimate failure state is characterized (for the quasi-static and cyclic load case) considering the magnitude of stresses  $\sigma_{max}$  of the current load block  $n_b$ . Here, the basic idea of the above energy hypothesis ( $g_f^{st} = g_f^{fat}$ ) is applied. Based on the applied stress ratio  $R = \sigma_{min}/\sigma_{max}$ , the number of load cycles to failure  $N_f$  is determined in step 3 using constant life diagrams (see [5]). In step 4, the fatigue damage increase, represented by the fatigue strain evolution, is calculated based on the number of load cycles  $n_b$  applied virtually for the current load block. The shape of the strain evolution curves changes based on the load level. Thereby, it is assumed that the higher the load level, the faster the strain propagates. Finally, in steps 5 and 6, the updated degradation factors  $\eta_R$  and  $\eta_E$  for strength and stiffness, respectively, are determined iteratively by ensuring the balance of energies ( $g^{st} = g^{fat}$ ) for the set parameters  $\sigma_{max}$  and  $\varepsilon_{new}^{fat}$ .

For a realistic lifetime prediction under variable loading conditions, it is also crucial to capture the influence of passive damage effects, which occur under loading patterns with a change in load direction. Here, tensile-induced damage affects subsequent compressive-induced damage and vice versa. To account for these effects in the FDM analysis, the degradation factors contained in the model were coupled together to allow for exchange of the respective tensile and compressive damage components. At this point, it was assumed that the increase of degradation  $\Delta\eta^t$  caused under tensile load could be superposed on the degradation caused under compressive load  $\Delta\eta^c$  and vice versa. Figure 2 shows the coupling procedure of the tensile and compressive degradation factors, as considered in the FDM for passive damage. Based on the load characteristics of the current load block, a distinction was made between reversed ( $R < 0$ ) and non-reversed ( $R \geq 0$ ) cyclic loading. In case of reversed cyclic loading, the calculation procedure (according to Figure 1) was performed for both the tensile and the compressive part. If a non-reversed cyclic loading was present, the damage analysis was carried out only for the tensile (TT) or the compressive (CC) range and the newly calculated degradation factors were subsequently superposed with each other.

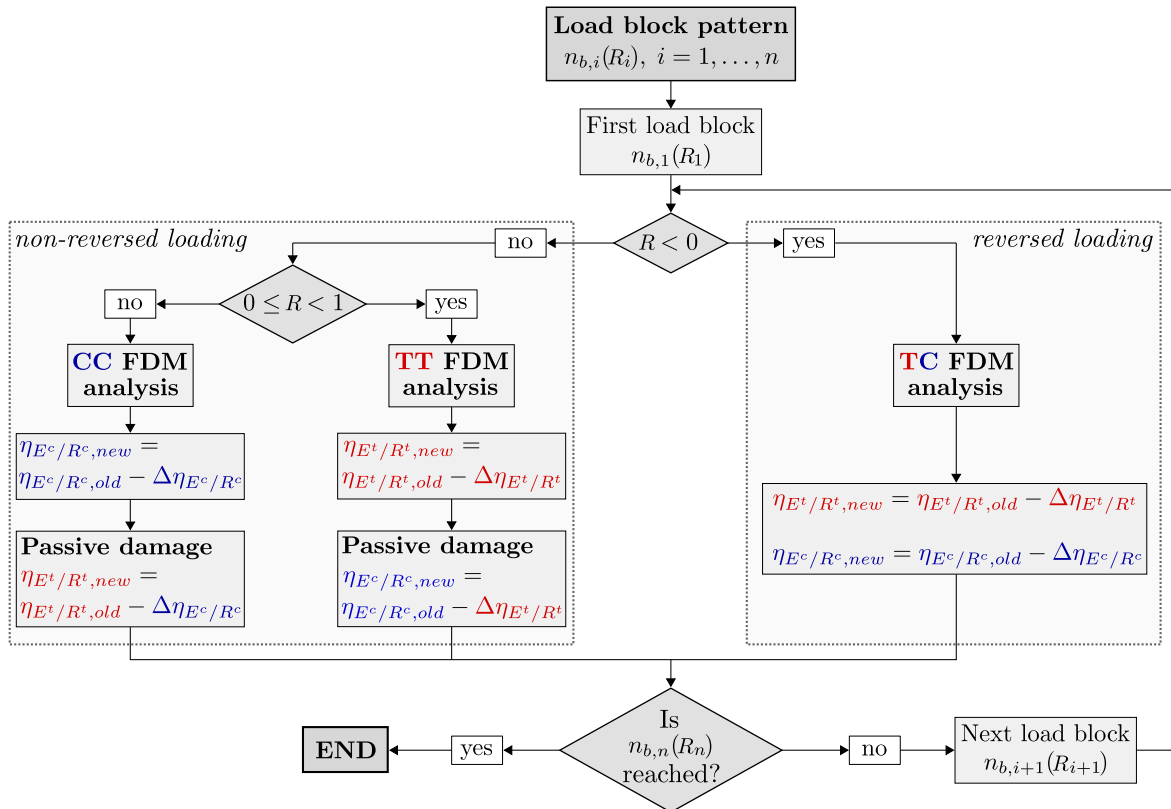


Figure 2. Flowchart illustrating the capture of passive damage effects in FDM analysis [6].

A detailed description of the FDM including all assumptions and mathematical expressions can be found in [3]. Details of model extensions to the FDM are described in [4–6].

### 3. LIFE PREDICTION UNDER VARIABLE BLOCK LOADING CONDITIONS

This section presents the conducted study on numerical fatigue analysis using the FDM under variable block loading conditions. Here, the overall objective was to assess the predictive accuracy of the model with respect to the capturing of load sequence and passive damage effects. The results presented below are part of an extensive investigation recently conducted by Brod et al. [6]. Figure 3 schematically shows the block loading patterns (hereinafter referred to as blocks), that were applied for the fatigue simulations. The load block characteristics were chosen based on the investigations of Adam et al. [8]. For the current study, six blocks with different load sequences were applied. According to Figure 3, each block consists of four load units (A, B, C, and D). In addition to blocks with only cyclic tensile load units (TTTT-1 and TTTT-2), blocks with a mixture of cyclic tensile and compressive load units (TCTT-1, TCTT-2, CCTC-1 and CCTC-2) were chosen. It should be noted that all tensile load units had a stress ratio of  $R = 0.1$ , and all compressive load units had a stress ratio of  $R = 10$ . Table 1 lists the associated load characteristics of the respective load units.

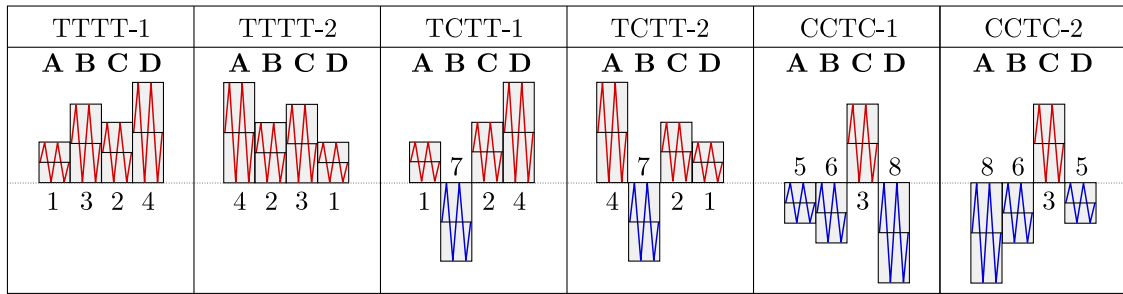


Figure 3. Definition of four-unit blocks for block loading simulations (based on [8]).

Table 1. Overview of peak stresses  $\sigma_{peak}$  and number of load cycles  $n_{unit}$  for each load unit.

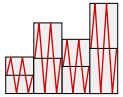
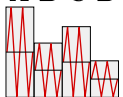
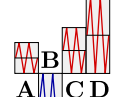
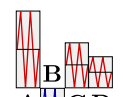
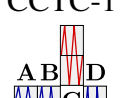
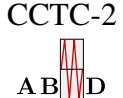
Unit	1	2	3	4	5	6	7	8
$\sigma_{peak}$ [GPa]	0.507	0.524	0.576	0.663	-0.325	-0.352	-0.386	-0.440
$n_{unit}$ [-]	162 574	29 256	4 016	231	162 576	29 257	4 016	231

For performance of the numerical calculations, the FDM was linked to a single fully integrated layered shell element (S4). Following the investigations of Adam et al. [8], a laminate stacking sequence of  $[(\pm 45/0_2)_2]_s$  with a nominal ply thickness of  $t^{ply} = 0.125$  mm was chosen. Furthermore, the FDM has been calibrated for T700SC/LY556 material (for details see [4]). To avoid a time-consuming and computationally intensive cycle-by-cycle analysis, the simulations were carried out with four calculation steps per load unit  $n_{unit} = 4 \cdot n_{b,FDM}$ .

In Table 2, the simulation results determined by the FDM are compared with those determined from experimental tests by Adam et al. [8]. In each case, the comparison is based on the num-

ber of repeating blocks and the specific load unit at which the respective failure was detected. Furthermore, for each test result, the number of load cycles to failure  $N_f$  and the corresponding average values  $\varnothing N_f$  are also indicated.

Table 2. Comparison of predicted (FDM) and experimentally [8] determined fatigue failure.

Load pattern	FDM			Experiments [8]				
	Blocks	Unit	$N_f$	Test No.	Blocks	Unit	$N_f$	$\varnothing N_f$
TTTT-1 A B C D 	4	D	784 077	1	6	D	1 176 347	914 831
				2	4	D	784 070	
				3	4	D	784 078	
				4	9	D	1 764 510*	
				5	9	D	1 647 462*	
TTTT-2 A B C D 	4	A	588 404	1	14	A	2 549 003*	637 307
				2	5	A	784 308	
				3	4	A	588 231	
				4	4	A	588 342	
				5	4	A	588 347	
TCTT-1 A B C D 	2	B	360 659	1	2	A	202 742	380 142
				2	2	D	392 110	
				3	2	B	358 691	
				4	2	B	359 056	
				5	3	D	588 111	
TCTT-2 A B C D 	2	B	197 312	1	9	B	1 568 887*	197 101
				2	2	A	196 243	
				3	2	B	196 396	
				4	1	D	196 077	
				5	2	B	199 689	
CCTC-1 A B C D 	1	D	195 961	1	1	D	195 920	195 860
				2	1	D	195 846	
				3	1	D	195 839	
				4	1	D	195 850	
				5	1	D	195 849	
CCTC-2 A B C D 	2	A	196 077	1	3	B	398 294	309 211
				2	2	A	196 276	
				3	2	D	363 215	
				4	2	A	196 086	
				5	3	A	392 186	

\* – Outlier test; not considered in average value  $\varnothing N_f$

Table 2 shows that the calculated failure points of all TTTT blocks occurred after four repe-

titions at the highest stress amplitude. In addition, the TTTT-1 block with increasing stress amplitude achieved a longer lifetime than the TTTT-2 block with decreasing amplitude. Similar to the TTTT blocks, the same load sequence effect was observed for the TCTT blocks. The TCTT-2 block with decreasing stress amplitude showed a shorter lifetime than the TCTT-1 block with increasing amplitude. Furthermore, the influence of the compressive load units was clearly noticeable. Compared to the TTTT blocks, the TCTT blocks showed significantly lower fatigue life. Here, all calculated fatigue failure states already occurred after two repetitions at the compressive load unit. When comparing the CCTC with the TTTT and the TCTT blocks, a different failure behavior was observed. The CCTC-1 block with increasing stress amplitude failed earlier than the CCTC-2 block with decreasing amplitude. However, the magnitude of the load sequence effect covered by the FDM was less pronounced for the CCTC compared to the TTTT and TCTT blocks. Comparing the simulation results of all TTTT, TCTT and CCTC blocks with the listed experimental data, good agreements could be found. Additionally to Table 2, Figure 4 shows the laminate residual strength curves  $R_{x,da}^{lam}/R_{x,0}^{lam}$  calculated with the FDM based on the number of load cycles (for details see [6]).

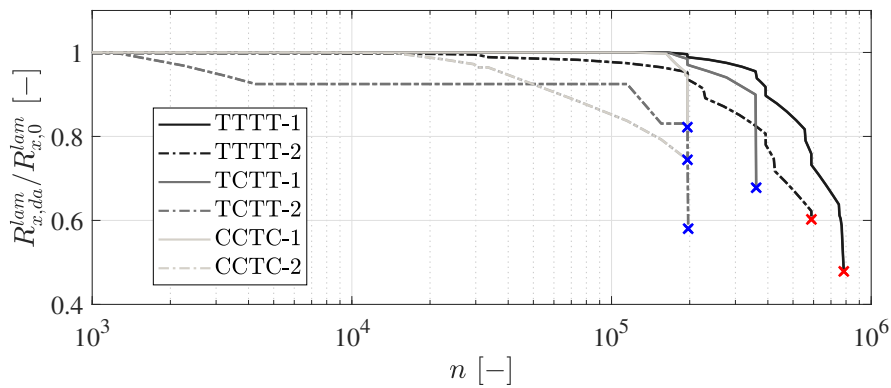


Figure 4. Predicted residual strength behavior of the block loading investigations.

Finally, the fatigue life  $N_f$  predicted by the FDM was compared to that using the linear Miner sum  $M$  for the block loading patterns. This comparison is intended to show the magnitude of the error in the damage measure when using linear damage accumulation rules for FRP components. The Miner sum  $M$  used is defined as follows [8]:

$$M = \sum_{i=1}^k \left( \frac{n_{b,A}}{N_{f,A}} \right)_i + \sum_{i=1}^k \left( \frac{n_{b,B}}{N_{f,B}} \right)_i + \sum_{i=1}^k \left( \frac{n_{b,C}}{N_{f,C}} \right)_i + \sum_{i=1}^k \left( \frac{n_{b,D}}{N_{f,D}} \right)_i \leq 1, \quad (2)$$

where  $n_{b,m}$  is the number of load cycles of the partial load blocks and  $N_{f,m}$  is the number of load cycles to failure of the respective load units  $m = \{A,B,C,D\}$ . Table 3 summarizes the results and shows the relative errors  $e_{i/j} = \frac{N_{f,i} - N_{f,j}}{N_{f,j}}$  between the FDM and experiments ( $e_{FDM/exp}$ ), Miner's Sum and experiments ( $e_{M/exp}$ ), as well as Miner's Sum and FDM ( $e_{M/FDM}$ ). Comparing

the listed results, it is evident that the errors  $e_{i/j}$  of Miner's sum become larger the higher the nonlinear damage evolution is. This becomes particularly obvious when considering the TCTT and CCTC blocks. The FDM, by contrast, provides consistently reliable results, with a tendency toward a slightly conservative lifetime prediction, when compared with the experiments.

Table 3. Comparison of obtained lifetimes by means of FDM (nonlinear damage accumulation), Miner's sum  $M$  (linear damage accumulation), and experiments.

Load pattern	$\varnothing N_{f,exp} [-]$	$N_{f,FDM} [-]$	$N_{f,M} [-]$	$e_{FDM/exp} [\%]$	$e_{M/exp} [\%]$	$e_{M/FDM} [\%]$
TTTT-1	914 831	784 077	980 385	-14.3	+7.2	+25.0
TTTT-2	637 307	588 404	980 385	-7.7	+53.8	+66.6
TCTT-1	380 142	360 659	980 385	-5.1	+157.9	+171.8
TCTT-2	197 101	197 312	980 385	+0.1	+397.4	+396.9
CCTC-1	195 860	195 961	980 385	+0.1	+400.6	+400.3
CCTC-2	309 211	196 077	980 385	-36.6	+217.1	+400.0

#### 4. FATIGUE DAMAGE ANALYSIS OF A BLENDED WING BODY FUSELAGE SHELL

This section aims to demonstrate that the FDM is also suitable for fatigue analysis of structural applications. For this purpose, a FRP fuselage shell of a blended wing body (BWB) aircraft was chosen as use case. In Figure 5(a), the basic structure of the associated FE-model as well as an illustrative BWB concept <sup>1</sup> is shown. It should be noted that this BWB fuselage segment model is a result of a preliminary design study performed by Bishara et al. [9]. A description of structural components provided in the fuselage segment, as well as their individual function is presented in [9]. The structural analysis considered only the outer FRP shell examined for possible fatigue damage was considered, since it has to withstand the high bending loads transferred from the wings. Thereby, the shell was modeled exemplarily as a quasi-isotropic laminate with a stacking sequence of  $[90/\pm 45/0]_s$ . In this relation, as composite material T700SC/LY556 was applied, identical to the investigations in Section 3. Furthermore, the FE-model included layered shell elements with three integration points per layer across the shell thicknesses. As load spectrum, the standardized TWIST block loading pattern [10] developed for transport aircraft was applied for bending loading (see Figure 5(c) and Table 4). Figure 5(b) shows schematically how the bending load was transferred to the structure. The model was simplified to a beam fixed at one end and simply supported at the other end. The loads were introduced into the fuselage segment via the reference points (RP) RP 1 and RP 2. Here, RP 1 and RP 2 were connected to the upper and lower edges of the outer shell, respectively via kinematic constraints. It is worth mentioning in this context that no boundary conditions were chosen at the front and back sides of the fuselage model, which means that the internal forces transmitted in the longitudinal direction were neglected (for details see [9]).

<sup>1</sup>Boeing advanced BWB concept, [https://commons.wikimedia.org/w/index.php?title=File:Boeing\\_advanced\\_blended\\_wing\\_body\\_concept\\_2011.jpg&oldid=520079306](https://commons.wikimedia.org/w/index.php?title=File:Boeing_advanced_blended_wing_body_concept_2011.jpg&oldid=520079306) (accessed 16 June 2021).



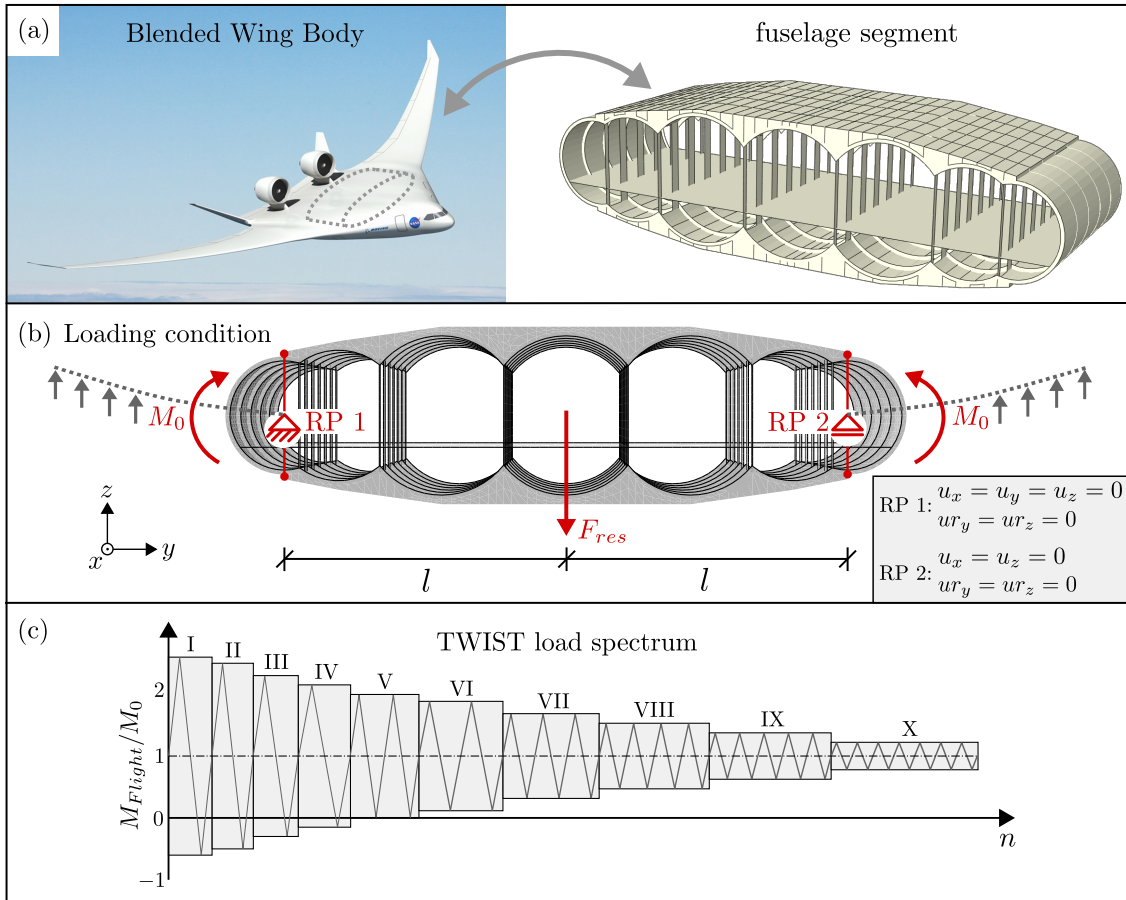


Figure 5. (a) Concept design<sup>1</sup> of a BWB aircraft (left) and FE model of the fuselage segment [9] (right); (b) Boundary conditions and applied bending load on BWB fuselage model; (c) Transport Wing Standard (TWIST) [10] load spectrum for numerical fatigue analyses.

The so-called mean static bending load  $M_0$  (see Figure 5(b)), which served as the reference value for the applied TWIST load spectrum, was calculated based on a BWB design and optimization study conducted by Liu et al. [11]. Using the simplified mechanical assumption that the BWB aircraft in flight was considered as a beam fixed at one end and simply supported at the other end, the moment  $M_0$  transferred to the fuselage structure was calculated as follows:

$$M_0 = \frac{F_{res} \cdot l}{2} = \frac{m_{tow} \cdot g \cdot l}{2} = \frac{132.000 \text{ kg} \cdot 9.81 \text{ m/s}^2 \cdot 6.25 \text{ m}}{2} = \underline{\underline{4046625 \text{ Nm}}}, \quad (3)$$

where  $g$  is the gravity acceleration,  $F_{res}$  is the resultant weight force at the center of mass of the fuselage segment, and  $l$  is the distance from the center of mass to the respective RP. Furthermore,  $m_{tow}$  is the maximum takeoff weight of the BWB, which was determined by Liu et al. [11]. It must be explicitly mentioned that the calculated load  $M_0$  represents a very rough assumption and is a purely fictitious value. The cyclic bending loads at flight stage

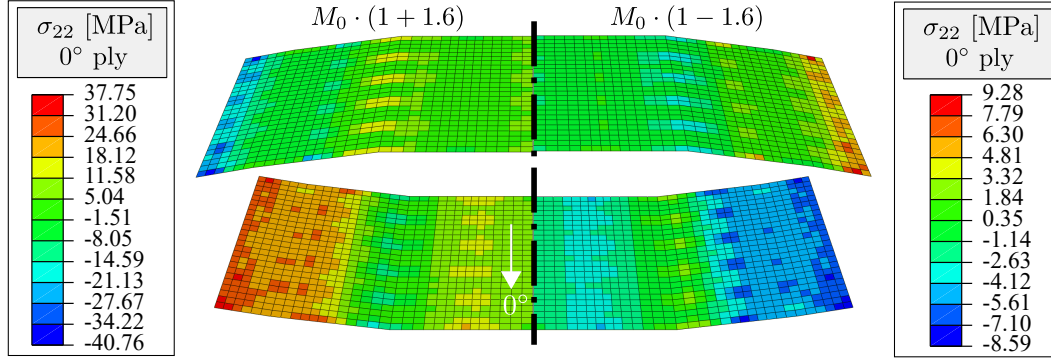
$M_{Flight}$  were obtained by multiplying the load factors (LF) given in Table 4 by the load  $M_0$ :  
 $M_{Flight} = M_0 \cdot (1 \pm LF)$ .

Table 4. Overview of the load levels of the TWIST load spectrum [10].

Load level	Load factor $LF$ [-]	Stress ratio $R$ [-]	Load cycles $n$ [-]
I	$\pm 1.6$	-0.23	10
II	$\pm 1.5$	-0.20	20
III	$\pm 1.3$	-0.13	50
IV	$\pm 1.15$	-0.07	180
V	$\pm 0.995$	0.00	520
VI	$\pm 0.84$	0.09	1 520
VII	$\pm 0.685$	0.19	8 000
VIII	$\pm 0.53$	0.31	41 700
IX	$\pm 0.375$	0.45	348 000
X	$\pm 0.222$	0.64	3 586 650

The numerical simulations presented in Figure 6 were performed for two different block loading pattern to demonstrate that the FDM is also capable of capturing load sequence effects at structural level. Thereby, the TWIST load spectrum shown in Figure 5(c) was applied in original (high  $\rightarrow$  low sequence) and reversed (low  $\rightarrow$  high sequence) orders. Figure 6(a) shows the local stress components of the outer shell, when the maximum and minimum bending load  $M_{Flight} = M_0 \cdot (1 \pm 1.6)$  was present. As expected, the highest stresses were induced at the transition region from the wings to the fuselage. Above this, locally excessive stresses occur in the outer shell caused by the perpendicular webs (see Figure 5(a)). In the remaining area the stresses decayed to a lower level and were distributed over the surface. The results of the fatigue analyses are summarized in Figure 6(b). As an example, the predicted matrix-induced stiffness degradation is shown in the  $0^\circ$  ply. Also, the calculated damage pattern of the high  $\rightarrow$  low is compared with the low  $\rightarrow$  high TWIST load sequence. Looking at the determined damage patterns, the induced damage can be seen especially at the transition from the wings to the fuselage shell. Additionally, low local stiffness reductions were detected in the vicinity of the web regions. This seems plausible considering the local high stresses at these locations (see Figure 6(a)). When comparing the high  $\rightarrow$  low with the low  $\rightarrow$  high TWIST load sequence, it was also noticeable that the load sequence with increasing stress amplitudes induced less damage, in contrast to the case with decreasing stress amplitudes. Reasons for this phenomenon were stress redistributions, the strain evolution curves implemented in the FDM and the chosen laminate layup, which changed their shape depending on the applied load level (see Section 2. ). It can be summarized that the present use case has demonstrated that the FDM is potentially applicable for damage analysis of structural applications. Although the results shown can be considered plausible, extensive validation work still needs to be performed to better assess the quantity of model predictions.

(a) Stress component  $\sigma_{22}$  in  $0^\circ$  ply at  $M_{Flight}$



(b) Predicted stiffness degradation in  $0^\circ$  ply

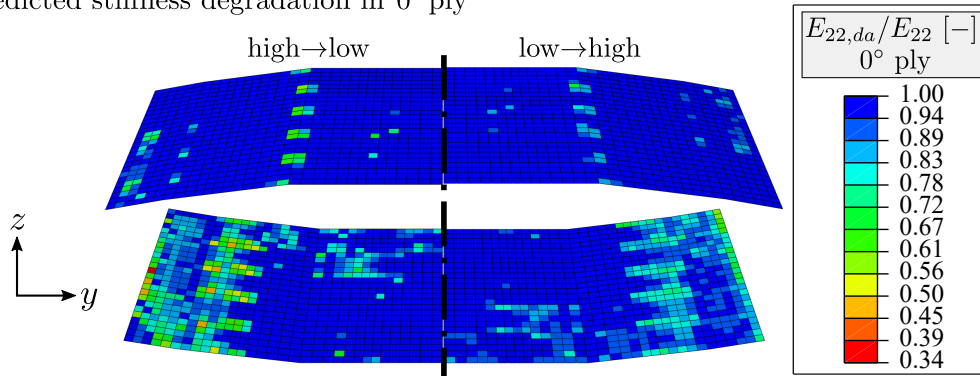


Figure 6. (a) Local  $\sigma_{22}$  stress distribution in  $0^\circ$  ply at  $M_{Flight} = M_0 \cdot (1 \pm 1.6)$ ; and (b) predicted stiffness degradation in  $0^\circ$  layer of outer shell for different load sequences: (left) original TWIST (high  $\rightarrow$  low sequence), and (right) reversed TWIST (low  $\rightarrow$  high sequence).

## 5. CONCLUDING REMARKS

In this contribution, a progressive fatigue damage model (FDM) was proposed and employed for fatigue analysis of fiber reinforced plastics (FRP) under variable block loading conditions. In the first part, the functionality of the FDM and the modeling features related to variable loading conditions were described. In the second part, results of a numerical fatigue study on multidirectional laminates considering different block loading patterns were presented. It was demonstrated that the FDM accurately accounts for the load sequence and passive damage effects typical for FRP. At the same time, the comparison with experimental findings proved the model validity. On that basis, in the last part of this contribution, the FDM was applied to fatigue analysis on a structural use case. In this context, simulations were performed on an FRP outer shell of a future blended wing body fuselage segment under development using a standardized aircraft load spectrum. The calculation results achieved through the FDM were found to be plausible. Nevertheless, in future it is required to carry out extensive validation work at the structural level using experimental tests.

## Acknowledgement

The authors gratefully acknowledge the financial support of the German Research Foundation (DFG) within the Projects 281870175 and 457043708.

## References

- [1] R. Talreja, N. Phan (2019) Assessment of damage tolerance approaches for composite aircraft with focus on barely visible impact damage. *Composite Structures*, **219**, 1–7.
- [2] A. P. Vassilopoulos (2019) Fatigue Life Prediction of Composites and Composite Structures (Second Edition). *Woodhead Publishing*.
- [3] H. Krüger, R. Rolfes (2015) A physically based fatigue damage model for fibre-reinforced plastics under plane loading. *International Journal of Fatigue*, **70**, 241–251.
- [4] M. Brod, G. Just, A. Dean, E. Jansen, I. Koch, R. Rolfes, Gude (2019) Numerical modelling and simulation of fatigue damage in carbon fibre reinforced plastics at different stress ratios. *Thin-Walled Structures*, **139**, 219–231.
- [5] M. Brod, A. Dean, S. Scheffler, C. Gerendt, R. Rolfes (2020) Numerical Modeling and Experimental Validation of Fatigue Damage in Cross-Ply CFRP Composites under Inhomogeneous Stress States. *Composites Part B: Engineering*, **200**, 108050.
- [6] M. Brod, A. Dean, R. Rolfes (2021) Numerical Life Prediction of Unidirectional Fiber Composites under Block Loading Conditions using a Progressive Fatigue Damage Model. *International Journal of Fatigue*, **147**, 106159.
- [7] D. Pfanner (2003) Zur Degradation von Stahlbetonbauteilen unter Ermüdungsbeanspruchung. Ph.D. Thesis, Ruhr Universität Bochum, VDI-Verlag, Germany.
- [8] T. Adam, N. Gathercole, H. Reiter, B. Harris (1994) Life prediction for fatigue of T800/5245 carbon-fibre composites: II. Variable-amplitude loading. *International Journal of Fatigue* **1994**, *16* (8), 533–547.
- [9] M. Bishara, P. Horst, H. Madhusoodanan, M. Brod, B. Daum, R. Rolfes (2018) A structural design concept for a multi-shell Blended Wing Body with laminar flow control. *Energies*, **11**(2), 383.
- [10] J. De Jong, D. Schütz, H. Lowak, J. Schijve (1973) A standardized load sequence for flight simulation tests on transport aircraft wing structures. *Nationaal Lucht-en Ruimtevaartlaboratorium*, NLR-TR 73029 U, LBF Bericht FB-106.
- [11] Y. Liu, A. Elham, P. Horst, M. Hepperle (2018) Exploring vehicle level benefits of revolutionary technology progress via aircraft design and optimization. *Energies*, **11**(1), 166.